Development of a space-borne spectrometer to monitor atmospheric ozone

Yury S. Dobrolenskiy,[1,2,*] Dmitry V. Ionov,[3] Oleg I. Korablev,[1,2] Anna A. Fedorova,[1,2] Evgeny A. Zherebtsov,[4] Andrey E. Shatalov,[4] Sergey N. Mantsevich,[1,5] Denis A. Belyaev,[1,2] Nikita A. Vyazovetskiy,[1] Pavel P. Moiseev,[4] Konstantin N. Tchikov,[6] Valery M. Krasavtsev,[6] Alexander V. Savushkin,[7] Dmitry M. Rumyantsev,[6] Igor V. Kananykhin,[6] Alexey I. Viktorov,[4] Alexey V. Kozyura,[4] Sergey A. Moryakin,[4] and Anatoly V. Poberovskii[3]

[1]Space Research Institute of Russian Academy of Sciences, Moscow, Russia

[2]Moscow Institute of Physics and Technology (State University), Dolgoprudny, Russia

[3]Faculty of Physics, St. Petersburg State University, St. Petersburg, Russia

[4]Scientific Production Enterprise "Astron Electronics," Orel, Russia

[5]Faculty of Physics, M. V. Lomonosov Moscow State University, Moscow, Russia

[6]St. Petersburg National Research University of Information Technologies, Mechanics and Optics, St. Petersburg, Russia

[7]S. I. Vavilov State Optical Institute, St. Petersburg, Russia

*Corresponding author: dobrolenskiy@iki.rssi.ru

Received 29 October 2014; revised 12 February 2015; accepted 2 March 2015; posted 10 March 2015 (Doc. ID 225922); published 8 April 2015

A new compact satellite spectrometer dedicated to monitoring terrestrial atmospheric ozone (ozonometer) is in preparation for the Russian Geophysics Program. Four instruments at four satellites (*Ionosphere*) are intended to monitor the total ozone content by measuring spectra of scattered solar radiation in nadir. The spectrometer is based on the Rowland scheme with a concave holographic diffraction grating. It covers the near UV and visible range of the spectrum, 300–500 nm, with a spectral resolution of ~0.3 nm. At present, a qualification model has been manufactured and tested. We introduce the description of the instrument and the results of laboratory and ground-based atmospheric calibrations. The ozone amount retrieved from atmospheric measurements using the differential optical absorption spectroscopy (DOAS) method is in good agreement with that measured by the collocated Brewer spectrophotometer and ozone monitoring instrument on board the *Aura* satellite.

OCIS codes: (010.0280) Remote sensing and sensors; (010.4950) Ozone; (230.1950) Diffraction gratings; (300.6190) Spectrometers; (300.6170) Spectra; (120.6085) Space instrumentation.

http://dx.doi.org/10.1364/AO.54.003315

1. Introduction

Ozone is responsible for the absorption of ultraviolet (UV) solar radiation between 0.2 and 0.4 μm. There are two ozone absorption bands in this range: the Hartley band (about 200–300 nm with maximum at 255 nm) and the Huggins band (300–360 nm). Absorption in the Hartley band is very intense, so that radiation at wavelengths less than 280–290 nm is totally absorbed by the ozone layer. Absorption in the Huggins band is also strong but not as strong as in the Hartley band, and solar radiation at wavelengths higher than 300 nm partly reaches the terrestrial

1559-128X/15/113315-08$15.00/0

surface. Thus, it is the Huggins band that is most commonly used for ozone nadir measurements from spacecraft. Ozone has also a weak absorption band system in visible light, at wavelengths between 375 and 600 nm (Chappuis bands). Visible light reaches the surface, so these bands are often used for ground-based ozone monitoring [1].

Satellite observations of the reflected UV–visible radiation allow us to monitor the global distribution of ozone content. Continuous measurements of this kind have been carried out since the 1970s: Total Ozone Mapping Spectrometer (TOMS [2]), Global Ozone Monitoring Experiment (GOME and GOME-2 [3,4]), SCanning Imaging Absorption spectroMeter for Atmospheric CHartographY (SCIAMACHY [5]), and the Ozone Monitoring Instrument (OMI [6–8]). At present, two instruments—OMI launched in 2004 and GOME-2 launched in 2008—provide daily global coverage of the Earth, delivering ozone data almost in real time. Nevertheless, such instruments have a limited lifetime, rarely exceeding 10 years, so the redundancy in ozone measurements and timely replacement of dedicated equipment are recommended by the international community.

In this paper, we introduce a new satellite spectrometer operating in the UV–visible range to monitor Earth's ozone layer, which is being developed within a Russian federal task program, Geophysics. The program is mostly dedicated to ionosphere and magnetosphere investigation, and its satellites are not optimized for optical observations. Nevertheless, the goal of total ozone monitoring has been considered important, and dedicated pencil-beam instruments were included in the payload. Up to now, the qualification prototype of the instrument has been designed and tested. To fit the mission constraints, we had to develop a compact instrument. Despite the low mass and simplicity, the ozonometer has demonstrated the capability to measure the total ozone column with good accuracy. It is also possible to retrieve NO_2 content from the measurements in the visible range of light. We present the description of the instrument and the results of laboratory and ground-based atmospheric calibrations.

2. Space Program Geophysics and the Ozonometer Experiment

The aim of the Russian federal task program Geophysics, planned to launch approximately in 2016-2017, is to develop a network of ground-based and space-borne instruments to monitor multiple geophysical parameters. In the context of the program, a group of five near-Earth satellites, *Ionozond*, is to be launched for monitoring ionosphere, magnetosphere, and solar activity as well as the processes in the neutral atmosphere, including dynamics of atmospheric ozone. This orbital group will consist of four satellites, *Ionosphere*, to primarily monitor the status of the ionosphere, and one satellite, *Zond*, dedicated mostly to the observations of the Sun (Fig. 1). The *Ionosphere* satellites are planned to

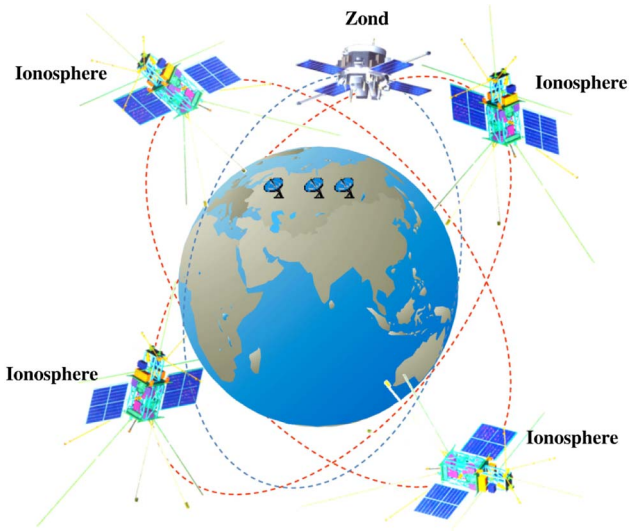

Fig. 1. Orbital group *Ionozond*.

be launched into a pair of circular near-polar (inclination 98°) sun-synchronous mutually orthogonal orbits, with two satellites at each orbit. The orbit altitude at the equator is 820 km with a period 101.3 min. The ozone measurements were considered as a useful complement for this geophysical mission, and a simple instrument to monitor the atmospheric ozone was recommended for inclusion in the payload of each of the four spacecraft. The ozonometer is, therefore, designed as a simple pencil-beam instrument. The spacecraft allows pointing in a nadir with an accuracy of 0.5° and stability 0.01°/s. With an instantaneous field of view (IFOV) of 0.02° × 0.22° and typical value of exposure time of 1 s, the spatial resolution on the ground will be 8 × 3 km (along × across track). The measurements are to be performed on dayside of the orbit, thus observing narrow stripes on the globe. The distance between the adjacent stripes will be ~2800 km, or ~1400 km with the two satellites. A somewhat loose coverage of the globe is achieved each day. Table 1 illustrates the main parameters of the mission and the ozonometer instrument.

The operation of the instrument includes three main regimes: survey (looking toward **–Z** through the main window), dark current calibration, and Sun calibration (through the window on the top cover). Dark current calibration is planned at each orbit on the nightside, while Sun calibration is planned only at each 10th orbit. Figure 2 shows the exterior view of the ozonometer with the axes of the spacecraft: **v** is velocity vector, **–Z** identifies the nadir direction, and **Y** marks the Sun hemisphere. A photo of the ozonometer instrument is shown in Fig. 3.

The fifth satellite, *Zond*, will be delivered to a special orbit, also circular, near-polar, and sun-synchronous with the following parameters: altitude at the equator 650 km, inclination 97°, period 98 min. A larger mass budget of this satellite allows using a more sophisticated scanning instrument to measure

Table 1. Main Parameters of the Ozonometer Experiment for *Ionosphere* Satellites

Parameter	Value
Spectral range, nm	300–500
Spectral resolution, nm	0.3
IFOV, along × across trajectory, degrees	0.02 × 0.22
Pixel size on Earth's surface, along × across trajectory (at exposure time 1 s), km × km	8 × 3
Range of exposure times, ms	50–4000
Entrance objective	
Type	Off-axis parabolic mirror
Effective light diameter, mm	38
Focal length, mm	132
Slit dimensions, μm × μm	40 × 500
Diffraction grating	
Type	Holographic concave (spherical)
Radius of curvature, mm	250
Groove density, mm^{-1}	533
Reciprocal linear dispersion, nm/mm	7.3
Detector	
Type	Dalsa IL-C6-2048C
Number of pixels	2048
Pixel size, μm × μm	13 × 500
Maximal sensitivity, $V/(\mu J/cm^2)$	360
Maximal readout frequency, MHz	25
Orbit	
Type	Circular, near-polar, sun-synchronous
Inclination	98°
Altitude at the equator, km	820
Period, min	101,3
Dimensions, cm × cm × cm	34 × 25 × 11
Mass, kg	6

ozone in an extended spectral range with a ground resolution of 10 × 10 km and swath of about 800 km. This development will be described in a separate paper.

3. Optical Scheme

The basic optical scheme of the spectrometer is based on the Rowland circle and is close to the

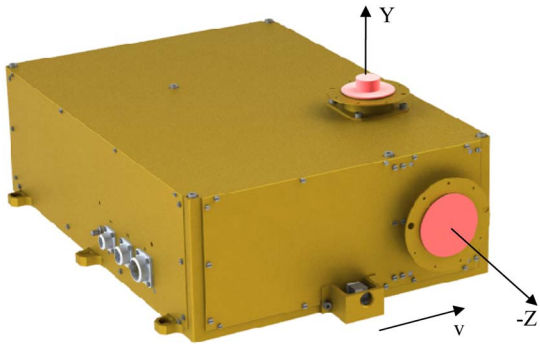

Fig. 2. Exterior view of ozonometer: **v** is velocity vector of the spacecraft; **–Z** is nadir direction; and **Y** marks the Sun hemisphere.

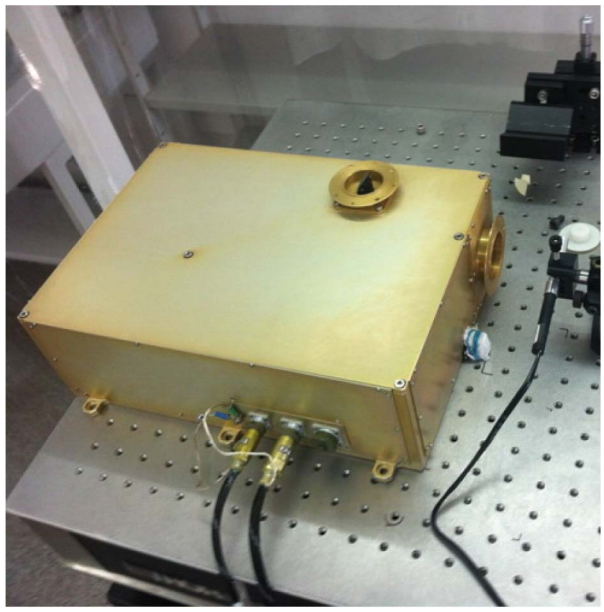

Fig. 3. Ozonometer during optical test with Hg lamp.

Paschen–Runge mount [9,10]. The entrance slit of the spectrometer, the diffraction grating, and the detector are located on the circumference known as the Rowland circle. A concave grating with a radius of curvature twice of the radius of the Rowland circle, i.e., equal to the Rowland circle diameter, forms the spectrum on the same circle. The advantage of the concave grating is that it also serves as a focusing element, eliminating the need in collimator and camera objectives. This allows reducing the number of optical elements, which is particularly important in the UV range. Concave gratings are widely used in the spectrometers for UV and visible light, including those used for atmospheric and space research [1,11,12]. On the other hand, concave grating spectrometers suffer from high astigmatism, originating from the fact that only the meridional focus (for the rays in the dispersion plane) is located on the Rowland circle, while the sagittal focus (for the rays in the plane orthogonal to the plane of the dispersion) is located beyond the circle. Even though for atmospheric observations the quality of the footprint is not very important, astigmatism leads to energy losses when part of the light escapes the detector. If the entrance slit and the detector have a significant height (in the direction perpendicular to the plane of dispersion), the effect of spectral line curvature may hamper the spectral resolution (e.g., see [12]).

To decrease the astigmatism and other aberrations, one can use a toroidal grating with different radii of curvature in the meridional and sagittal planes. This allows bringing the sagittal focus closer to the meridional one, thus reducing astigmatism. A similar result may be obtained using the holographic method of grating manufacture. The holographic method gives much more opportunities in obtaining individual required characteristics of a grating. With

the ozonometer, we use a custom-made spherical holographic grating produced by the State Institute of Applied Optics. The grating belongs to the so-called second-type holographic grating, produced by illuminating the photoresist with a divergent light from two point sources of the wavelength at 441.6 nm. It operates in the first diffraction order and is optimized for the spectral region of 0.3–0.5 μm, having the minimum of astigmatism at 365 nm. The radius of curvature is 250 mm, optical dimensions are 50×50 mm, and the groove density is 533 grooves/mm.

The optical scheme of the ozonometer is shown in Fig. 4. Solar radiation reflected from Earth's surface and scattered by Earth's atmosphere comes from the nadir direction and is incident to the instrument's entrance window (1) made of quartz glass. Passing through the optical aperture baffle (2), it meets the parabolic mirror (3) used as an entrance objective. The mirror is off-axis with an effective light diameter of 38 mm and focal length of 132 mm. Being reflected from the parabolic mirror and after that from the folding mirror (4), which is used for optimizing the instrument size, light is focused on the spectrometer's slit (5). The dimensions of the slit are 500×40 μm, forming the IFOV of $0.22° \times 0.02°$. A special element (6) mounted in front of the slit serves to depolarize the incident light. The problem is that optical performance of a grating spectrometer (and first of all the diffraction efficiency) depends on polarization of the incident light [9,10]. To avoid this effect with the polarized light from the atmospheric scattering, special polarization measurement devices (PMD) were used in similar instruments [3,5]. Such polarization measurements can be rather complicated and need accurate interpretation [13]. Instead, we used another approach similar to one used in the OMI experiment: depolarizer of incident light comprising four wedged quartz plates with different orientation of their optical axes [7]. As a result, the instrument becomes independent of light polarization.

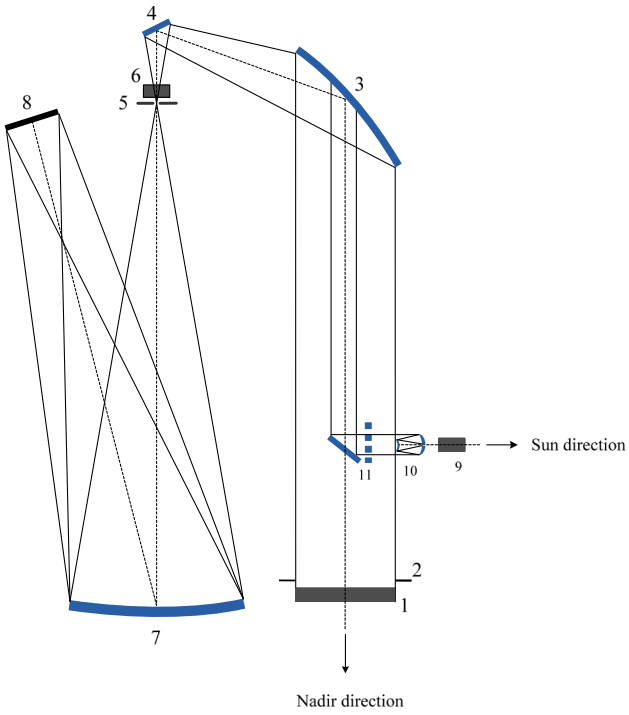

Fig. 4. Optical scheme of ozonometer: 1, entrance window; 2, aperture baffle; 3, parabolic mirror; 4, folding mirror; 5, slit; 6, depolarizer; 7, grating; 8, detector; calibration channel: 9, milk glass cylinder; 10, two-mirror objective; 11, two-position mirror.

After the slit, the light beam goes to the grating (7) at an incidence angle of $\psi = 0$ (normal incidence). Such an arrangement makes it possible to direct the nondiffracted light (the zero order) backward through the slit, thus reducing the stray light on the detector. In the case of normal incidence and for the first diffraction order, the diffraction angles are determined from the following expression:

$$\varphi_\lambda = \arcsin \frac{\lambda}{d}, \tag{1}$$

where φ_λ is the diffraction angle for the wavelength λ and d is the period of grating. The reciprocal linear dispersion in this case can be found as follows:

$$\frac{d\lambda}{dl} = \frac{d \cos \varphi_\lambda}{r}, \tag{2}$$

where r is grating's radius of curvature, i.e., diameter of the Rowland circle. For our grating, we have $d\lambda/dl \approx 7.3$ nm/mm, changing slightly within the range of 0.3–0.5 μm. The spectrum formed by the grating is focused on the linear CCD detector (8).

The optical scheme and general opto-mechanical design can be also seen in Fig. 5, showing the interior view of the instrument.

In order to measure the out-of-atmosphere solar spectra, a special calibration channel with a separate optical entrance oriented toward the Sun is included (see Fig. 4). In orbit, the sun may be observed in a number of directions within the 40°–60° interval in

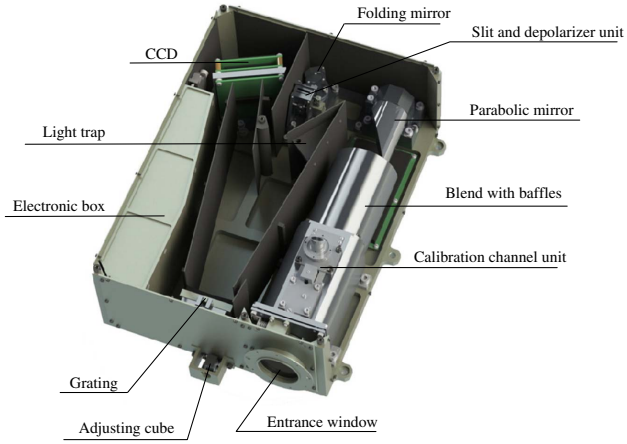

Fig. 5. Interior view of ozonometer.

the YZ plane from the Y axis toward Z. The channel consists (Fig. 4) of a milk glass cylinder (9) providing approximately equal light flux at different positions of the Sun, two-mirror objective (10) with a hole in big mirror, and a two-position flipping mirror (11) directing light onto the main parabolic mirror. During regular nadir observations, the flipping mirror is closed (this position is shown by the dashed line). During Sun calibrations, it opens (shown as the solid line), and the sunlight is directed into the instrument. Simultaneously, the main entrance window 1 is closed with the help of an optical shutter nearby the entrance window (not shown in Fig. 4). A milk glass cylinder is a piece of milk (opal) quartz glass of cylindrical form. Its input facet is oblique to be normal to the rays coming from the "mean position" of the Sun during calibrations. The side facet of the cylinder is enclosed into the housing of aluminum working as a mirror to prevent light from leaving the cylinder through the side facet and to increase the "scattering" properties of the element by reflections. Laboratory tests showed no narrow spectral features originating from this cylinder; nevertheless, the level of signal is rather low, so this channel may be modified later on. The design of the calibration channel and switching mechanism in its present form is shown in Fig. 6.

As for the dark current calibration, a small shutter located in front of the slit is used, which shuts any light propagating through the slit to the grating and further to the detector.

4. Detector

The dispersed spectrum is registered by the photodetector, which is a CCD-array Dalsa IL-C6-2048C (see Table 1). The array has 2048 pixels, forming spectral sampling of ~0.1 nm/pixel. The pixel size is 13×500 μm, while the slit size is 40×500 μm. Thus, the image of the slit corresponds to 3 pixels

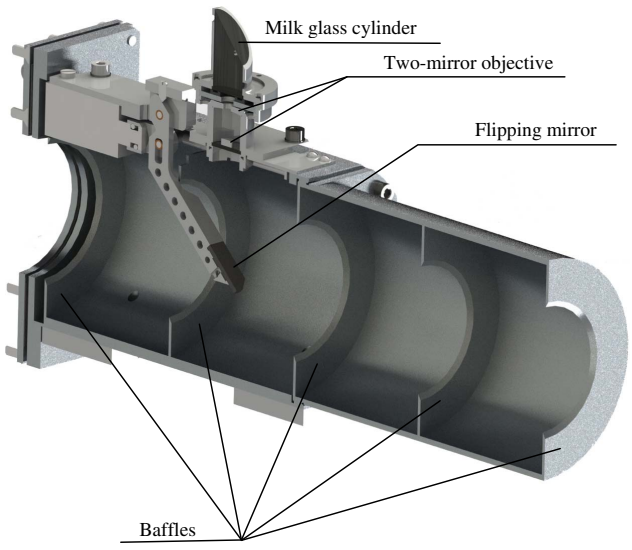

Fig. 6. Design of the calibration channel and switching mechanism.

forming a spectral resolution of 0.3 nm. This resolution is a bit better than what is generally required for the ozone measurements in the near UV. Higher values would not result in higher accuracy (one needs a higher signal-to-noise ratio in that case) but would probably need another detector with more pixels, which would, in turn, lead to higher requirements to compensate aberrations and finally to more complicated optical design. For the processing of the analog signal from the CCD array, the signal processor is used that provides binary correlation sampling and analog–digital conversion (ADC) with 12 bit capacity. Root-mean-square deviation of noise at the output of the processor is 1.2 of least significant bit. The measured dynamic range of the whole detector unit, including noise of CCD, amplifier, and ADC, is near 55 dB.

The exposure time of the detector is limited by the dark current: the larger exposure time, the larger part of the dynamic range is "filled" by the dark signal. For example, at the detector temperature of 5°C, the dark current is about 500 ADU (analog–digital units) for the exposure time 0.5 s and about 2000 ADU for the exposure time 2 s. The dark signal increases linearly with exposure time and proportionally to a square of detector temperature. The estimates of required in-flight exposure times, which follow the instrument aperture and detector sensitivity, are within 1–2 s, but during twilight longer times are needed. So the longer the possible exposure time for the instrument, the higher values of solar zenith angle (SZA) are acceptable.

The detector is cooled by the Peltier cooler. The design range of the instrument base temperature is from −10°C to +40°C. During the laboratory tests, we managed to cool the detector down to 35° relatively to the mounting face of the instrument in a vacuum or down to 28° in air. For example, for the temperature in a vacuum chamber of 20°C, we achieved the detector temperature of −15°C. This also made it possible to operate with longer exposure times (up to 4 s).

Assuming the nominal detector temperature of 0°C and a typical exposure time of 1–2 s, the estimated signal-to-noise ratio is in the range of 500–1200. This is better than required for the retrieval of an ozone vertical column from the space measurements in UV, which is about 200–300 (e.g., see [14]).

5. Laboratory Tests

Laboratory tests with a mercury lamp were carried out in order to estimate the spectral resolution and to obtain the wavelength calibration of the spectrometer. A spectrum of a mercury lamp has a number of narrow lines with well-known wavelengths. We have used an ORIEL 6034 Hg–Ne pen-ray lamp. Figure 7 shows the mercury lamp spectrum measured by ozonometer. Considering the width of the lines to be much narrower than the slit function of the instrument, we measured FWHM for the four

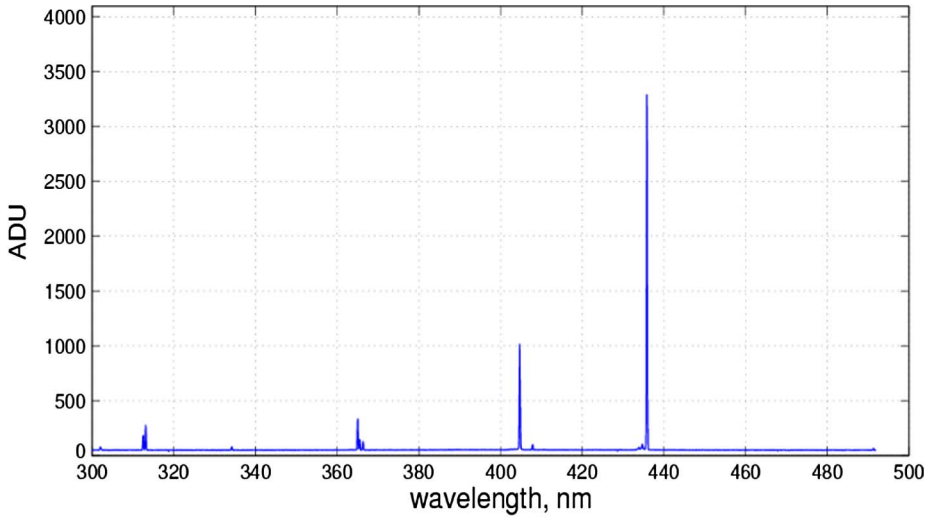

Fig. 7. Spectrum of mercury lamp measured by ozonometer.

most bright mercury lines in this range: 313.17, 365.02, 404.66, and 435.84 nm (see Fig. 7). For all these lines, the FWHM is approximately 0.3 nm. Two close lines of the UV triplet with wavelengths 365.02 and 365.48 nm are clearly resolved. All the peaks in Fig. 7 were identified with mercury line atlases (e.g., a weak peak on the very left is 302.15 nm line) to be sure they are not "ghosts" or other undesired signals. On the base of this spectrum, the wavelength calibration was obtained fitting the positions of the lines by a second-degree polynomial function. The following expression was obtained for the wavelength dependence on pixel number:

$$\lambda[nm] = 296.708 + 0.095n + 0.000000479n^2, \quad (3)$$

where λ is the wavelength corresponding to the pixel number n. The second-order term of Eq. (3) is very small, indicating slow changing of the grating's linear dispersion in the range 300–500 nm. It is known, however [9], that if the exit slit (or detector plane) of a monochromator is oriented perpendicularly to the diffracted beam (not exactly tangentially to the Rowland circle), the linear dispersion would be constant. For the case of a spectrograph with a linear detector, it is not possible to satisfy this condition for all points of the detector, so the nonlinearity will always take place. The optimal approximation is given by Eq. (3), showing that in our case the nonlinearity is quite low.

As mentioned above, diffraction efficiency of a grating depends (and in some cases rather strongly) on the polarization state of an incident light wave. Such dependencies were observed for grating-based spaceborne spectrometers [7,13]. The dependency of the measurement result on the polarization of the input radiation was checked using a polarizer placed between the lamp and the instrument entry. In Fig. 8, one can see the fragment of the same mercury spectrum as in Fig. 7 measured with two mutually orthogonal planes of light polarization. The red curve corresponds to the P plane of polarization (parallel to grating's grooves, TE mode), while the blue curve corresponds to the S plane of polarization (perpendicular to grating's grooves, TM mode). The spectra at the upper panel were measured when the depolarizer was removed from the scheme. It

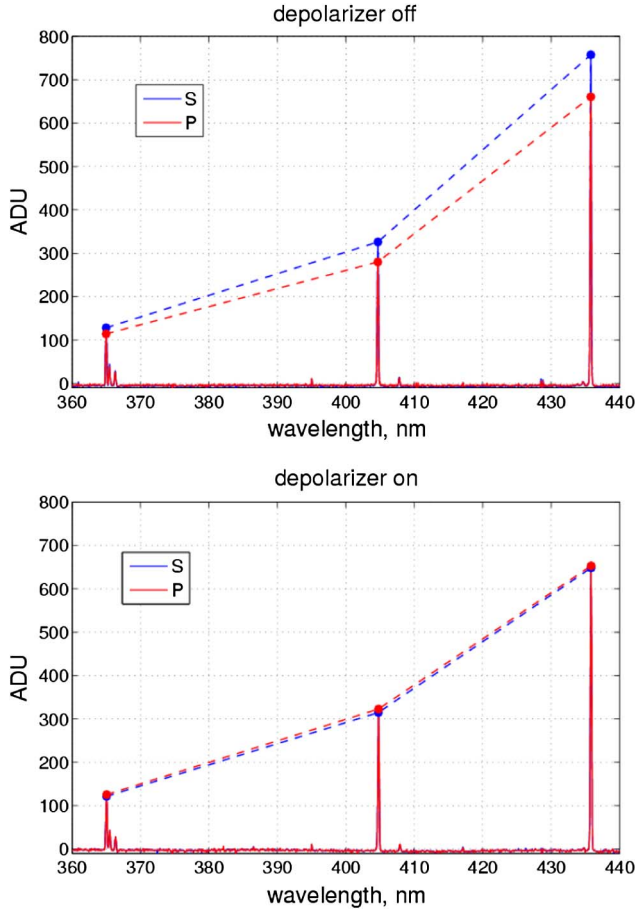

Fig. 8. Mercury spectrum (the same as in Fig. 7) but measured in polarized light for two states of polarization without (top) and with (bottom) the depolarizing element.

is clearly seen that the S-mode signal on the detector is higher than for P mode, and this difference increases slightly with the wavelength. This result is in agreement with diffraction gratings theory [9,10], predicting, in general, a higher diffraction efficiency for the S mode (although there may be singular points). However, the polarization sensitivity of the ozonometer is not as high as reported for OMI [7]. The bottom panel shows the same spectra measured in full instrument configuration, including the depolarizer. In this case, the difference in signal on the detector for different polarization modes approaches the noise level and should be negligible for data processing.

6. Field Observations and Interpretation

To assess practical capabilities of the instrument to measure the atmospheric ozone, zenith-sky ground-based observations of scattered solar radiation were carried out at Kislovodsk High Mountain Scientific Station (KHMS, 2070 m.a.s.l.) on December 2012 with the qualification prototype of the ozonometer. Direct Sun observations (with the instrument entrance window oriented toward the Sun) were also performed, but further analysis and total ozone retrieval are based on zenith-sky measurements. In spite of the wintertime, location of the site (~43.7°N) allowed us to observe in a wide range of daytime sun elevations, SZA varying from ~66° at noon to ~87° at sunset. During the 6 h observations, ~1000 valid zenith spectra were acquired, with exposure times varying from 1 to 4 s.

Estimation of total ozone (vertical column) content in the atmosphere is done by comparing the spectra registered at substantially different sun elevations. Two example spectra, corresponding to minimum and maximum SZA observed, are shown in Fig. 9. These spectra could not be compared directly, as they were measured under different conditions of registration (exposure time, detector cooling, etc.), and the accurate absolute calibration is missing. Nevertheless, one may notice a significantly suppressed

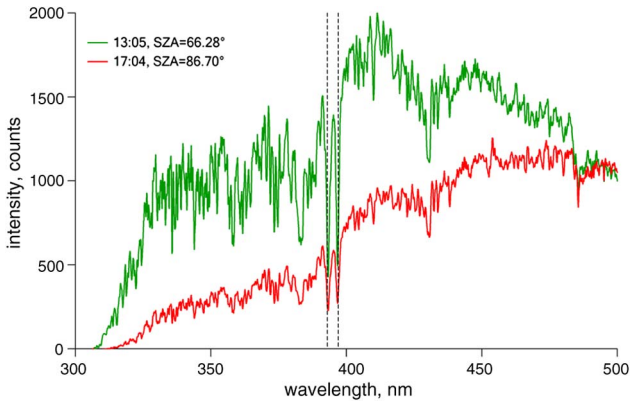

Fig. 9. Spectra of zenith-sky scattered solar radiation, registered at KHMS (Kislovodsk) on 6 December 2012, measured at high and low sun. Vertical dashed lines mark Fraunhofer lines of ionized calcium at 393 and 397 nm.

UV radiation in the evening, compared to daytime observations. Both spectra reveal easily recognizable Fraunhofer lines of ionized calcium at 393 and 397 nm, marked with vertical dashed lines. The signal-to-noise ratio of these measurements is estimated as ~100 for the spectra acquired at ~87° SZA and ~200 for the spectra acquired at ~66° SZA.

Acquired spectra of the scattered light were analyzed with the help of well-known DOAS (differential optical absorption spectroscopy, [15]) technique using the WinDOAS software [16] developed at Belgium Institute of Space Aeronomy (BIRA-IASB). WinDOAS is accustomed for the processing of DOAS observations within the international Network for the Detection of Atmospheric Composition Change (NDACC, [17]). A DOAS algorithm is commonly used in such type of field experiments (e.g., see [14]). A detailed description of total ozone retrieval with the help of the DOAS technique is beyond the scope of the present paper. Total ozone amount estimated from these 1000 spectra turned out to be 312 ± 4 Dobson Units (DU). This value is in good agreement with the data of Brewer spectrophotometer measurements (included in World Ozone and Ultraviolet Radiation Data Centre [18]) carried out at the same location on the same day, 311 ± 2 DU. For comparison, according to the data of satellite measurements by Aura OMI instrument, total ozone value in the vicinity of Kislovodsk was ~313 DU on that day [19].

7. Conclusion

Qualification prototype of a new lightweight satellite UV–visible spectrometer to monitor atmospheric ozone in the UV range has been designed and tested. The optical design of the instrument is based on Rowland circle scheme with concave aberration-reduced diffraction grating. Laboratory tests and calibrations showed spectral resolution up to 0.3 nm and good optical performance. The observations collocated with Brewer spectrophotometer were carried out at Kislovodsk High Mountain Station, resulting in a one-day series recorded in December 2012. The resulting value of the ozone vertical column retrieved using DOAS algorithm is in good agreement with the measurements of a collocated Brewer spectrophotometer and satellite data (OMI), demonstrating adequate measurement capabilities of the prototype.

The authors acknowledge the hospitality and support from the team at the Kislovodsk High Mountain Station of the A. M. Obukhov Institute of Atmospheric Physics of Russian Academy of Sciences and, in particular, Vladimir Savinykh for his help and useful discussion. The work of authors affiliated with MIPT is supported by the Ministry of Education and Science of Russian Federation (Grant No.: 11.G34.31.0074 and project 8413).

References

1. J.-P. Pommereau and F. Goutail, "O_3 and NO_2 ground-based measurements by visible spectrometry during arctic winter and spring 1988," Geophys. Res. Lett. **15**, 891–894 (1988).

2. D. F. Heath, A. J. Krueger, H. R. Roeder, and B. D. Henderson, "The solar backscatter ultraviolet and total ozone mapping spectrometer (SBUV/TOMS) for Nimbus 7," Opt. Eng. **14**, 144323 (1975).
3. J. P. Burrows, M. Weber, M. Buchwitz, V. V. Rozanov, A. Ladstätter-Weißsenmayer, A. Richter, R. DeBeek, R. Hoogen, K. Bramstedt, K.-U. Eichmann, and M. Eisinger, "The global ozone monitoring experiment (GOME): mission concept and first scientific results," J. Atmos. Sci. **56**, 151–175 (1999).
4. R. Munro, M. Eisinger, C. Anderson, J. Callies, E. Corpaccioli, R. Lang, A. Lefebvre, Y. Livschitz, and A. P. Albinana, "GOME-2 on Metop: from in-orbit verification to routine operations," in *EUMETSAT Meteorological Satellite Conference*, Helsinki, Finland, 12–16 June 2006.
5. H. Bovensmann, J. P. Burrows, M. Buchwitz, J. Frerick, S. Noël, V. V. Rozanov, K. V. Chance, and A. P. H. Goede, "SCIAMACHY: mission objectives and measurement modes," J. Atmos. Sci. **56**, 127–150 (1999).
6. P. F. Levelt, G. H. J. van der Oord, M. R. Dobber, A. Mälkki, H. Visser, J. de Vries, P. Stammes, J. O. V. Lundell, and H. Saari, "The ozone monitoring instrument," IEEE Trans. Geosci. Remote Sens. **44**, 1093–1101 (2006).
7. M. R. Dobber, R. J. Dirksen, P. F. Levelt, G. H. J. van der Oord, R. H. M. Voors, Q. Kleipool, G. Jaross, M. Kowalewski, E. Hilsenrath, G. W. Leppelmeier, J. de Vries, W. Dierssen, and N. C. Rozenmeijer, "Ozone monitoring instrument calibration," IEEE Trans. Geosci. Remote Sens. **44**, 1209–1238 (2006).
8. R. Dirksen, M. Dobber, R. Voors, and P. Levelt, "Prelaunch characterization of the ozone monitoring instrument transfer function in the spectral domain," Appl. Opt. **45**, 3972–3981 (2006).
9. V. V. Lebedeva, *Experimental Optics* (Faculty of Physics of M. V. Lomonosov Moscow State University, 2005) (in Russian).
10. C. Palmer and E. Loewen, *Diffraction Grating Handbook* (Newport Corp., 2005).
11. J.-L. Bertaux, O. I. Korablev, S. Perrier, E. Quémerais, F. Montmessin, F. Leblanc, S. Lebonnois, P. Rannou, F. Lefèvre, F. Forget, A. A. Fedorova, E. Dimarellis, A. Reberac, D. Fonteyn, J. Y. Chaufray, and S. Guibert, "SPICAM on Mars express: observing modes and overview of UV spectrometer data and scientific results," J. Geophys. Res. **111**, E10S90 (2006).
12. J.-L. Bertaux, D. Nevejans, O. I. Korablev, E. Villard, E. Quémerais, E. Neefs, F. Montmessin, F. Leblanc, J. P. Dubois, E. Dimarellis, A. Hauchecorne, F. Lefèvre, P. Rannou, J. Y. Chaufray, M. Cabane, G. Cernogora, G. Souchon, F. Semelin, A. Reberac, E. van Ransbeek, S. Berkenbosch, R. Clairquin, C. Muller, F. Forget, F. Hourdin, O. Talagrand, A. V. Rodin, A. A. Fedorova, A. V. Stepanov, I. I. Vinogradov, A. V. Kiselev, Yu. K. Kalinnikov, G. Durry, B. Sandel, A. Stern, and J. C. Gérard, "SPICAV on Venus express: three spectrometers to study the global structure and composition of the Venus atmosphere," Planet. Space Sci. **55**, 1673–1700 (2007).
13. C. P. Tanzi and A. Aben, "Polarization measurements of the global ozone monitoring experiment," in *Optical Remote Sensing*, Santa Barbara, California, 22 June 1999, paper RWB2.
14. M. Dobber, R. Dirksen, R. Voors, G. H. Mount, and P. Levelt, "Ground-based zenith sky abundances and in situ gas cross sections for ozone and nitrogen dioxide with the Earth observing system Aura ozone monitoring instrument," Appl. Opt. **44**, 2846–2856 (2005).
15. U. Platt and J. Stuz, *Differential Optical Absorption Spectroscopy (DOAS), Principles and Applications* (Springer, 2008) [ISBN 978-3-540-21193-8].
16. C. Fayt and M. van Roozendael, *WinDOAS 2.1 Software User Manual* (Belgian Institute for Space Aeronomy, 2001) http://uv-vis.aeronomie.be/software.
17. Network for the detection of atmospheric composition change, http://www.ndacc.org.
18. World Ozone and Ultraviolet Radiation Data Centre (WOUDC), http://www.woudc.org.
19. Aura Validation Data Center, http://avdc.gsfc.nasa.gov.